A Comparison of Flexible Coupling Models for Updating in Rotating Machinery Response

A. T. Tadeo
UNICAMP - Universidade Estadual de Campinas
Department of Mechanical Design
Postal Box: 6051
13083-970 Campinas, SP. Brazil
abdon@fem.unicamp.br

K. L. Cavalca
UNICAMP - Universidade Estadual de Campinas
Department of Mechanical Design
Postal Box 6051
13083-970 Campinas, SP. Brazil
katia@fem.unicamp.br

This paper analyzes the effects of the mathematical models of flexible couplings in rotating mechanical systems in terms of their vibrational behavior. The residual unbalance of the coupled shafts is considered to be the main source of vibration in the rotating system. The moments and the frequencies of the forces, which result from these effects, are close to the natural frequencies of the mechanical system. Since the coupling is considered to be a flexible component in the power transmission system, it introduces a certain amount of mass, damping and stiffness to the system, influencing its natural frequencies. The present work shows the modeling of a mechanical rotor-bearing-coupling system, through the finite element method, used in this case to analyze the transverse vibrations of the system. Different modeling techniques were taken into account for this purpose. Such models are recommended for flexible couplings to analyze their influence on the natural frequencies of the system and on the unbalance response of the system. Afterwards, a model updating was carried out to fit the coupling stiffness and damping coefficients, using the minimum quadratic technique. Some sensitivity of the proposed models was observed in relation to the coupling parameters.
Keywords*: Flexible couplings, flexible rotor, bending vibrations, model updating, rotor dynamics*

Introduction

Flexible couplings are widely used in rotating machines for power transmission, and for allowing a certain degree of misalignment between shafts, considered co-axially coupled by the couplings.

One of the functions of the couplings is to compensate the inevitable misalignment present in the so-called co-axial shaft assembly that can be parallel, angular, axial, or even a combination of these. If the misalignment effect is not minimised by the coupling, some consequences, such as noise; vibration; power losses; wearing of the bearings and seals; and fatigue failure of the shafts or couplings can occur.

Couplings can be divided in two basic groups: the ones that present mechanical misalignment; and the ones that present bending misalignment, Gibbons (1976) (see [1]).

In mechanical systems, shaft unbalance is an important source of vibration. The lack of information about the forces and the bending moments generated in the coupling due to shaft misalignment hinders a deeper understanding of the coupling influence on the system. There are several preliminary researches ([2],[4],[7],[9]), that proposed equations to determine the forces and moments generated in the coupling. However, they focus on a particular type of coupling and present constant values of contact forces in relation to a certain degree of misalignment. Consequently, the nature and behaviour of these forces has not been fully established.

Nelson et McVaugh [6] suggested two simplified models to represent the couplings, which were used in the rotor-bearing-coupling system modelling by Tapia and Cavalca [8]; Kramer [3] also proposed two simplified models for the couplings: the first model was used to analyse the bending vibration of the rotor-bearing-coupling system by Sekhar et al [7]. Xu et al [9] analysed the vibrations of a motor-flexible coupling-rotor system using a sub-structuring method, in which the coupling is described using several nodes.

Paper accepted June, 2003. Technical Editor: José Roberto de França Arruda.

The present work tries to analyse and compare the simplified theoretical models of the couplings suggested by Kramer [3], and Nelson and Crandall [6], and also the traditional model of the coupling as a rigid disk. After that, a model updating applying the minimum quadratic technique was carried out on a system composed of two flexible shafts, two rigid disks, a flexible coupling and four hydrodynamic bearings.

Nomenclature

$u(Y,t)$, $v(Y,t)$ = translation motion functions, respectively in the X and Z directions
$\alpha(Y,t)$, $\beta(Y,t)$ = small rotations around the axes X and Z, respectively
$\{F_d\},\{F_p\}$ = unbalance and gravitational forces vectors acting on the disk
$\{\ddot{q}_i\},\{\dot{q}_i\}$ = acceleration and velocity vectors of the disk, respectively
$[Md]$, $[Gd]$ = mass and gyroscopic matrices of the disks
m, I_d, I_a = mass, diametrical moment of inertia and polar moment of inertia of the disk
φ_i $(i=1,...,4)$ = shape functions
$\{q_i\}$, $\{q_j\}$ = generalised co-ordinates of the shaft
$[Me],[Ge],[Ke]$ = mass matrix, gyroscopic matrix and stiffness matrix for a beam element
E = Young modulus (or elasticity modulus) of the shaft
I = polar moment of inertia of the cross section of the shaft
A, ρ, k = area of the cross section of the beam, the mass density, and the shearing factor of the beam, respectively
G = shear modulus of the beam.
$\{F_c\}$ = connecting forces in the bearings
$c_{XX},c_{ZZ},k_{XX},k_{ZZ}$ = equivalent damping and stiffness coefficients in X, Z directions
$c_{XZ},c_{ZX},k_{XZ},k_{ZX}$ = equivalent damping and stiffness cross-coupled coefficients of the bearings
Ω = rotational speed of the shaft
$\{F_{ex}\}$ = external forces vector acting on the coupling
$\{F_{con}\}$ = connecting forces vector acting on the disk, shaft and coupling, which are cancelled when the complete matrix of the system is assembled

[Ma], [Ga], = mass and gyroscopic matrices due to the coupling presence (Kramer's model)
[Ca], [Ka] = damping and stiffness matrices due to the coupling presence (Kramer's model)
(k_T) (k_R) = isotropic translational and rotational stiffness (Nelson and Crandall's model)
[Kt] [Ct]= stiffness and damping matrix of the coupling (Nelson and Crandall's model)
I_{mi}, I_{mj} = mass moments of inertia of the disks
Ip_{mi}, Ip_{mj} = polar mass moments of inertia for the disks
[M] = symmetrical mass matrix of the system, comprising rigid disks, beam elements and couplings
[G] = gyroscopic matrix
[C],[K] = damping and stiffness matrices of the system
{Fe} = vector of the external forces acting on the system

Theoretical Development

Rotor-Bearing-Coupling System

The mechanical system shown in Fig. 1 is composed of two flexible shafts and two rigid disks that represent the rotors of the system, a flexible coupling, and four hydrodynamic bearings. Only the bending vibrations of the system will be considered.

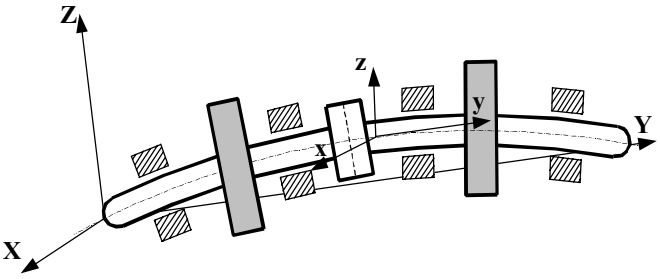

Figure 1. Rotating Rotor-Bearing-Coupling System.

The co-ordinates of the inertial reference system XYZ and the auxiliary reference system xyz (fixed to the shaft) are used to describe the equations of motion for each component of the system. Any cross section of the rotor is defined with respect to the XYZ system, by the translation motion functions u(Y,t), v(Y,t), respectively in the X and Z directions. These functions give the cross section centre position at a given time t. The orientation of this section is given by the small rotations $\alpha(Y,t)$, $\beta(Y,t)$ around the Z and X axes, respectively.

Components of the System

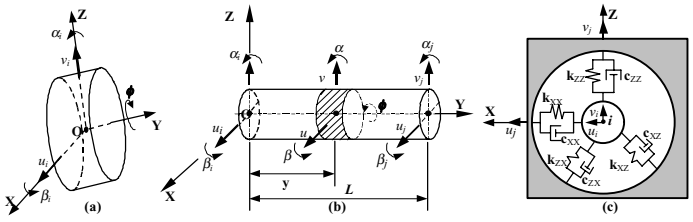

Figure 2. Finite Element Models: (a) Rigid Disk, (b) Flexible Shaft, (c) Hydrodynamic Bearings.

Rigid Disk

The equation of motion for the rigid disk [2], according to Fig. 2a, represented in the co-ordinate system XYZ, applying the Lagrange Equation, as developed by Lalanne [4] and Ehrich [1], considering a constant rotational speed Ω, is:

$$[\mathrm{Md}]\{\ddot{\boldsymbol{q}}_{\boldsymbol{i}}\} + \boldsymbol{\Omega}[\mathrm{Gd}]\{\dot{\boldsymbol{q}}_{\boldsymbol{i}}\} = \{\boldsymbol{F}_d\} + \{\boldsymbol{F}_p\} + \{\boldsymbol{F}_{con}\} \qquad (1)$$

where: $\{F_d\},\{F_p\},\{F_{con}\}$ are respectively, the unbalance, gravitational and connecting force vectors acting on the disk; $\{\ddot{\boldsymbol{q}}_{\boldsymbol{i}}\},\{\dot{\boldsymbol{q}}_{\boldsymbol{i}}\}$ are the acceleration and velocity vectors of the disk, respectively, and [Md], [Gd] are the sparse matrix of mass and gyroscopic matrix of the disks, for which the non-zero elements are defined as:

$$[\mathrm{Md}] = \mathrm{diag}[\mathrm{m} \quad \mathrm{m} \quad \mathrm{I_d} \quad \mathrm{I_d}] \;,\; \mathrm{Gd_{3,4}} = -\mathrm{Gd_{4,3}} = -\mathrm{I_a} \qquad (2)$$

Where: m, I_d, I_a are the mass, transverse moment of inertia and polar moment of inertia of the disk, respectively. The subscripts indicate the element location.

Shaft

The shaft was divided into beam elements of continuous mass and constant cross section [6], as presented in Fig. 2b. The co-ordinates of the translation motion u, v for the cross section are expressed in terms of the generalised co-ordinates of each element boundary through the following equation:

$$\begin{Bmatrix} u(y,t) \\ v(y,t) \end{Bmatrix} = \begin{bmatrix} \varphi_1 & 0 & 0 & \varphi_2 & \varphi_3 & 0 & 0 & \varphi_4 \\ 0 & \varphi_1 & -\varphi_2 & 0 & 0 & \varphi_3 & -\varphi_4 & 0 \end{bmatrix} \begin{Bmatrix} \{\boldsymbol{q}_{\boldsymbol{i}}\} \\ \{\boldsymbol{q}_{\boldsymbol{j}}\} \end{Bmatrix} \qquad (3)$$

Where: φ_i (i=1,...,4) are the shape functions which satisfy the boundary conditions; $\{q_i\}$, $\{q_j\}$ are the displacement vectors of the generalised coordinates of the shaft, and the rotational angles α,β represent the bending and are defined through the following mathematical relation, as well as the shear effects:

$$\begin{Bmatrix} \alpha(y,t) \\ \beta(y,t) \end{Bmatrix} = \begin{bmatrix} 0 & -\varphi'_1 & \varphi'_2 & 0 & 0 & -\varphi'_3 & \varphi'_4 & 0 \\ \varphi'_1 & 0 & 0 & \varphi'_2 & \varphi'_3 & 0 & 0 & \varphi'_4 \end{bmatrix} \begin{Bmatrix} \{\boldsymbol{q}_{\boldsymbol{i}}\} \\ \{\boldsymbol{q}_{\boldsymbol{j}}\} \end{Bmatrix} \qquad (4)$$

Where: φ'_i $(i = 1,..,4)$ are the derivatives of the shape functions φ_i.

Finally, the work and energy functions are expressed in terms of integrals along the beam element length, substituting the shape functions into the Lagrange Equations for a beam element of length L and radius r. The equation of motion, written by the element energy [1,4], for a constant rotational speed Ω is given by:

$$[\mathrm{Me}]\begin{Bmatrix} \{\ddot{\boldsymbol{q}}_{\boldsymbol{i}}\} \\ \{\ddot{\boldsymbol{q}}_{\boldsymbol{j}}\} \end{Bmatrix} + \Omega[\mathrm{Ge}]\begin{Bmatrix} \{\dot{\boldsymbol{q}}_{\boldsymbol{i}}\} \\ \{\dot{\boldsymbol{q}}_{\boldsymbol{j}}\} \end{Bmatrix} + [\mathrm{Ke}]\begin{Bmatrix} \{\boldsymbol{q}_{\boldsymbol{i}}\} \\ \{\boldsymbol{q}_{\boldsymbol{j}}\} \end{Bmatrix} = \begin{Bmatrix} \{\boldsymbol{F}_p\} \\ \{\boldsymbol{F}_{con}\} \end{Bmatrix} \qquad (5)$$

Where: the vectors $\{F_p\},\{F_{con}\}$ were defined for equation (1); [Me], [Ge] and [Ke] are the mass matrix, the gyroscopic matrix and the stiffness matrix for a beam element, respectively, defined as:

$$[\mathrm{Me}] = \begin{bmatrix} [\mathrm{m_{i,i}}] & [\mathrm{m_{i,j}}] \\ [\mathrm{m_{j,i}}] & [\mathrm{m_{j,j}}] \end{bmatrix} ; [\mathrm{Ge}] = \begin{bmatrix} [\mathrm{g_{i,i}}] & [\mathrm{g_{i,j}}] \\ [\mathrm{g_{j,i}}] & [\mathrm{g_{j,j}}] \end{bmatrix} ; [\mathrm{Ke}] = \begin{bmatrix} [\mathrm{k_{i,i}}] & [\mathrm{k_{i,j}}] \\ [\mathrm{k_{j,i}}] & [\mathrm{k_{j,j}}] \end{bmatrix} \qquad (6)$$

Notice that the sub-matrices are defined according to with the following mathematical relations presented by Nelson and Crandall:

$$[m_{i,i}] = \begin{bmatrix} u_1 & 0 & 0 & -u_2L \\ 0 & u_1 & u_2L & 0 \\ 0 & u_2L & u_3L^2 & 0 \\ -u_2L & 0 & 0 & u_3L^2 \end{bmatrix}$$

$$[m_{i,j}] = \begin{bmatrix} u_4 & 0 & 0 & u_5L \\ 0 & u_4 & -u_5L & 0 \\ 0 & u_5L & u_6L^2 & 0 \\ -u_5L & 0 & 0 & u_6L^2 \end{bmatrix} = [m_{j,i}]^T$$

$$[k_{i,i}] = \frac{EIL^{-3}}{1+12\phi} \begin{bmatrix} 12 & 0 & 0 & -6L \\ 0 & 12 & 6L & 0 \\ 0 & 6L & 4L^2(1+3\phi) & 0 \\ -6L & 0 & 0 & 4L^2(1+3\phi) \end{bmatrix}$$

$$[k_{i,j}] = \frac{EIL^{-3}}{1+12\phi} \begin{bmatrix} -12 & 0 & 0 & -6L \\ 0 & -12 & 6L & 0 \\ 0 & -6L & 2L^2(1-6\phi) & 0 \\ 6L & 0 & 0 & 2L^2(1-6\phi) \end{bmatrix} = [k_{j,i}]^T \quad (7)$$

$$[g_{i,i}] = \begin{bmatrix} 0 & -u_7 & -u_8L & 0 \\ u_7 & 0 & 0 & -u_8L \\ u_8L & 0 & 0 & -u_9L^2 \\ 0 & u_8L & u_9L^2 & 0 \end{bmatrix}$$

$$[g_{i,j}] = \begin{bmatrix} 0 & u_7 & -u_8L & 0 \\ -u_7 & 0 & 0 & -u_8L \\ -u_8L & 0 & 0 & u_{10}L^2 \\ 0 & -u_8L & -u_{10}L^2 & 0 \end{bmatrix} = -[g_{j,i}]^T$$

T is the superscript indicating the transpose of the matrix; ε is the shear coefficient of the shaft; E is the Young modulus (or elasticity modulus) of the shaft; I is the polar moment of inertia of the cross section of the shaft. Besides that, $[m_{i,i}]=[m_{j,j}]$, $[g_{i,i}]=[g_{j,j}]$ and $[k_{i,i}]=[k_{j,j}]$ except for the inverse signal of the terms 6L. The sub-matrices coefficients are defined as:

$$u_1 = (156 + 3528\varepsilon + 20160\varepsilon^2)\alpha_T + 36\alpha_R$$
$$u_2 = (22 + 462\varepsilon + 2520\varepsilon^2)\alpha_T + (3 - 180)\alpha_R$$
$$u_3 = (4 + 84\varepsilon + 504\varepsilon^2)\alpha_T + (4 + 60\varepsilon + 1440\varepsilon^2)\alpha_R$$
$$u_4 = (54 + 1512\varepsilon + 10080\varepsilon^2)\alpha_T - 36\alpha_R$$
$$u_5 = (13 + 378\varepsilon + 2520\varepsilon^2)\alpha_T - (3 - 180)\alpha_R$$
$$u_6 = -(3 + 84\varepsilon + 504\varepsilon^2)\alpha_T - (1 + 60\varepsilon - 720\varepsilon^2)\alpha_R \quad (8)$$

$$u_7 = 72\alpha_R \; ; \; u_8 = 2(3 - 180\varepsilon)\alpha_R \; ; \; u_9 = 2(4 + 60\varepsilon + 1440\varepsilon^2)\alpha_R$$
$$u_{10} = 2(1 + 60\varepsilon)\alpha_R$$

$$\alpha_T = \frac{\rho AL}{420(1+12\varepsilon)^2}, \alpha_R = \frac{\rho Ar}{120L(1+12\varepsilon)^2}$$

Where: A, ρ, ε are the cross section area, the mass density, and the shear factor of the beam, respectively. L is the length and r is the radius of the beam element. The shear effects are significant only at high rotational speeds.

Bearings

The model of the bearing used in the present work [1,4], as represented by Fig. 2c, neglects the influence of the rotation, the bending moments, and the oil film inertia effects. The governing equation for the bearing is given by:

$$\begin{bmatrix} \mathbf{c}_{XX} & \mathbf{c}_{XZ} \\ \mathbf{c}_{ZX} & \mathbf{c}_{ZZ} \end{bmatrix} \begin{Bmatrix} \dot{u}_i \\ \dot{v}_i \end{Bmatrix} + \begin{bmatrix} \mathbf{k}_{XX} & \mathbf{k}_{XZ} \\ \mathbf{k}_{ZX} & \mathbf{k}_{ZZ} \end{bmatrix} \begin{Bmatrix} \mathbf{u}_i \\ \mathbf{v}_i \end{Bmatrix} = \{\boldsymbol{F}_c\} \quad (9)$$

where, $\{F_c\}$ represents the connecting forces in the bearings; c_{XX},c_{ZZ},k_{XX},k_{ZZ} are the equivalent damping and stiffness coefficients in the X, Z directions, and c_{XZ},c_{ZX},k_{XZ},k_{ZX} are the equivalent damping and stiffness cross-coupled coefficients of the bearings. Finite Difference Method evaluated the values of the stiffness and damping coefficients and in this case their behaviour is practically constant for a rotational speed range of 2000 to 4000 rpm. The foundation degrees of freedom are neglected once the foundation is considered rigid. The values of the cross-coupled coefficients were very low and they were neglected to simplify the model updating, as suggested by Lalanne [4], considering that the main characteristics of the bearings link forces and displacements, neglecting the influence of slopes and bending moments.

Flexible Coupling

There is little information in literature about the best physical model of couplings to use, in order to improve their mathematical representation in mechanical systems. In general, when a coupling is modelled as a rigid body, the rigid disk model may be used in order to consider this component as an integrated part of the whole rotor-bearing-coupling system. However, this model neglects the flexibility of the coupling. The models of Kramer [3] and Nelson and Crandall [5] presented here, take into account the inherent flexibility of the couplings.

Kramer's Models

The first model suggested by Kramer [3], which considers the flexibility of mechanical couplings is defined as a non friction coupling that is rigid in the radial direction. In this model, the coupled shafts, as shown in Fig. 3a, are considered as the classical FEM with two beams with 8 degrees of freedom each. The coupling effect is to constrain the translation degrees of freedom in the i and j nodes (coupling position), making the translation motion in both nodes equal, $u_i=u_j$ and $v_i=v_j$,. In this way, the system, which initially had 16 degrees of freedom, was reduced to a system with 14 degrees of freedom, due to the presence of the coupling, as illustrated in Fig. 3b. The coupling mass must be added in the two nodes of the coupling as a rigid body (Sekhar et al (1996)).

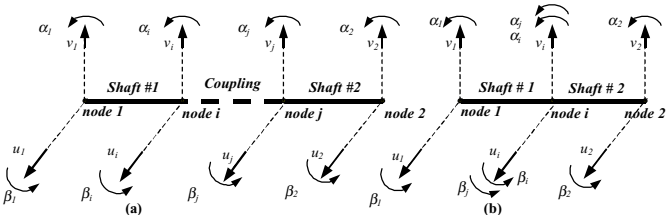

Figure 3. (a) Mechanical System of two shafts connected by a coupling, (b) First Kramer's Model of the System.

The second model suggested by Kramer [3], considers the rotational stiffness (kr) and damping (cr) of the coupling. But, in this case, the constraints of the first model are still maintained, and the system is represented by Fig. 4.

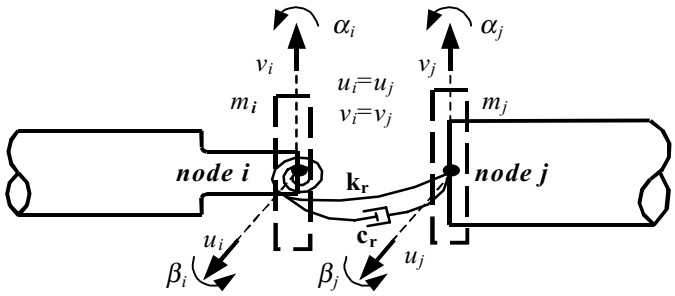

Figure 4. Second Kramer's Model for Flexible Coupling.

The equation of motion, for the coupling model of Fig. 4, can be written in the following way:

$$[\mathrm{Ma}]\begin{Bmatrix}\{\ddot{q}_i\}\\ \{\ddot{q}_j\}\end{Bmatrix} + [\Omega[\mathrm{Ga}] + [\mathrm{Ca}]]\begin{Bmatrix}\{\dot{q}_i\}\\ \{\dot{q}_j\}\end{Bmatrix} + [\mathrm{Ka}]\begin{Bmatrix}\{q_i\}\\ \{q_j\}\end{Bmatrix} = \{\mathrm{F_{ex}}\} + \{\mathrm{F_{con}}\} \tag{10}$$

where: $\{F_{con}\}$, $\{F_{ex}\}$ are the connecting and external force vector, respectively, acting on the coupling; [Ma], [Ga], [Ca], [Ka] are respectively, the mass, gyroscopic, damping and stiffness matrices due to the coupling (the mass and gyroscopic matrices are similar to those of the rigid disk). The sparse damping and stiffness matrices present the following non-zero elements:

$$\begin{aligned}&\mathrm{Ca}_{3,3} = -\mathrm{Ca}_{3,7} = \mathrm{Ca}_{4,4} = -\mathrm{Ca}_{4,8} = -\mathrm{Ca}_{7,3} = \mathrm{Ca}_{7,7} = -\mathrm{Ca}_{8,4} = \mathrm{Ca}_{8,8} = \mathbf{c_r},\\ &\mathrm{Ka}_{3,3} = -\mathrm{Ka}_{3,7} = \mathrm{Ka}_{4,4} = -\mathrm{Ka}_{4,8} = -\mathrm{Ka}_{7,3} = \mathrm{Ka}_{7,7} = -\mathrm{Ka}_{8,4} = \mathrm{Ka}_{8,8} = \mathbf{k_r},\\ &\mathrm{Ka}_{3,4} = -\mathrm{Ka}_{3,8} = -\mathrm{Ka}_{4,3} = \mathrm{Ka}_{4,7} = -\mathrm{Ka}_{7,4} = \mathrm{Ka}_{7,8} = \mathrm{Ka}_{8,3} = -\mathrm{Ka}_{8,7} = \boldsymbol{\Omega c_r}.\end{aligned} \tag{11}$$

Nelson and Crandall's Models

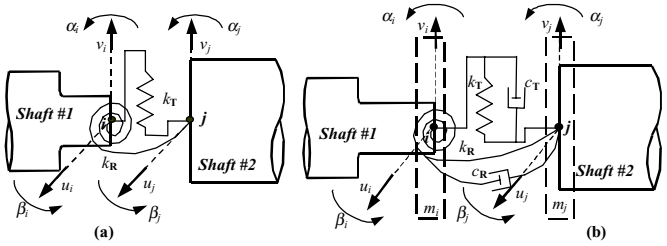

Figure 5. Nelson and Crandall's Models for Flexible Coupling: (a) with stiffness, (b) with stiffness and damping.

The first model defined by Nelson and Crandall [5] considers the coupling as an elastic component with isotropic translational (k_T) and rotational (k_R) stiffness, between the i and j stations, as shown by Fig. 5a. Under static conditions, the equation of motion of the coupling, is defined as:

$$[\mathrm{Kt}]\begin{Bmatrix}\{q_i\}\\ \{q_j\}\end{Bmatrix} = \{\mathrm{F_{con}}\} + \{\mathrm{F_{ex}}\} \tag{12}$$

where: $\{F_{con}\}$,$\{F_{ex}\}$ are the connecting forces and the external force vectors, acting on the coupling; [Kt] is the stiffness matrix of the coupling for which the non-zero elements are defined by equation (13).

$$\begin{aligned}&\mathrm{Kt}_{1,1} = -\mathrm{Kt}_{1,5} = \mathrm{Kt}_{2,2} = -\mathrm{Kt}_{2,6} = -\mathrm{Kt}_{5,1} = \mathrm{Kt}_{5,5} = -\mathrm{Kt}_{6,2} = \mathrm{Kt}_{6,6} = \mathrm{k_T}\\ &\mathrm{Kt}_{3,3} = -\mathrm{Kt}_{3,7} = \mathrm{Kt}_{4,4} = -\mathrm{Kt}_{4,8} = -\mathrm{Kt}_{7,3} = \mathrm{Kt}_{7,7} = -\mathrm{Kt}_{8,4} = \mathrm{Kt}_{8,8} = \mathrm{k_R}\end{aligned} \tag{13}$$

The second model suggested by Nelson and Crandall [5] considers, besides the coupling stiffness, the internal damping and the inertia effects of the coupling as well. The inertia effects are included in the model as two rigid disks at each connection station. Under these conditions, the physical model of the coupling is shown in Fig. 5b, and the equation of motion is written as follows:

$$[\mathrm{Ma}]\begin{Bmatrix}\{\ddot{q}_i\}\\ \{\ddot{q}_j\}\end{Bmatrix} + [\Omega[\mathrm{Ga}] + [\mathrm{Ct}]]\begin{Bmatrix}\{\dot{q}_i\}\\ \{\dot{q}_j\}\end{Bmatrix} + [\mathrm{Kt}]\begin{Bmatrix}\{q_i\}\\ \{q_j\}\end{Bmatrix} = \{\mathrm{F_{con}}\} + \{\mathrm{F_{ex}}\} \tag{14}$$

In equation (14), the mass matrix [Ma], the gyroscopic matrix [Ga], and the damping matrix [Ct] of the coupling present non-null elements defined as:

$$[\mathrm{Ma}] = \begin{bmatrix}\mathrm{m_i} & \mathrm{m_i} & \mathrm{I_{mi}} & \mathrm{I_{mi}} & \mathrm{m_j} & \mathrm{m_j} & \mathrm{I_{mj}} & \mathrm{I_{mj}}\end{bmatrix}$$

$$\mathrm{Ga}_{3,4} = -\mathrm{Ga}_{4,3} = -\mathrm{I_{pmi}}, \mathrm{Ga}_{7,8} = -\mathrm{Ga}_{8,7} = -\mathrm{I_{pmj}}; \tag{15}$$

$$\begin{aligned}&\mathrm{Ct}_{1,1} = -\mathrm{Ct}_{1,5} = \mathrm{Ct}_{2,2} = -\mathrm{Ct}_{2,6} = -\mathrm{Ct}_{5,1} = \mathrm{Ct}_{5,5} = -\mathrm{Ct}_{6,2} = \mathrm{Ct}_{6,6} = \mathrm{c_T},\\ &\mathrm{Ct}_{3,3} = -\mathrm{Ct}_{3,7} = \mathrm{Ct}_{4,4} = -\mathrm{Ct}_{4,8} = -\mathrm{Ct}_{7,3} = \mathrm{Ct}_{7,7} = -\mathrm{Ct}_{8,4} = \mathrm{Ct}_{8,8} = \mathrm{c_R}.\end{aligned}$$

Where: m_i, m_j are the coupling masses at the i and j stations; I_{mi}, I_{mj} , the mass moments of inertia of the disks, and Ip_{mi}, Ip_{mj} , the polar mass moments of inertia for the rigid disks at i and j stations.

These last two physical models defined by Nelson and Crandall [5] correspond to a model of discrete mass of the coupling, in which too small values of translational and rotational stiffness coefficients represent quasi flexible connections while higher stiffness values represent rigid connections.

Equation of Motion

The Direct Stiffness Method (DSM) [5] was applied to evaluate the stiffness coefficients for the beam elements of the model. Once the equations of motion are established for each component of the rotor-bearing-coupling system, the assembly of the complete equation of motion of the system was accomplished, as given by equation (16).

$$[\mathrm{M}]\{\ddot{q}\} + [\boldsymbol{\Omega}[\mathrm{G}] + [\mathrm{C}]]\{\dot{q}\} + [\mathrm{K}]\{q\} = \{\mathrm{F_e}\} \tag{16}$$

In this equation, [M] is the symmetrical mass matrix of the system, comprising of rigid disks, beam elements and couplings; [G] is the gyroscopic matrix which contains the same components as those of the mass matrix, and it depends on the rotation Ω of the shaft; [C] and [K] are the dissipative and stiffness matrices of the system. The [C] and [K] matrices can be symmetric for isotropic bearings, or even non-symmetric when the bearings are anisotropic and their coefficients depend on the rotation Ω; and {Fe} is the vector of the external forces acting on the system.

Natural Frequency Analysis

An exponential solution of equation (16) is assumed in the form $\{q\}=\{q_o\}e^{\lambda t}$ in the time domain. The solution is substituted into equation (16), which has to be previously reduced to a first order differential homogeneous equation. Consequently, the corresponding eingenvalue problem is defined by equation (17).

$$\left[\lambda\begin{bmatrix}[0] & [M]\\ [M] & [\Omega[G]+[C]]\end{bmatrix}+\begin{bmatrix}-[M] & [0]\\ [0] & [K]\end{bmatrix}\right]\{q_o\}=\{0\} \qquad (17)$$

Since the matrices order [M], [K], [G], [C] are nxn, the solution of equation (17) results in 2n complex eingenvalues (λ) for each rotational speed Ω. The Campbell Diagram can be obtained solving equation (17) in a range of rotational speed values. In this way, it is possible to obtain a set of eigenvalues (natural frequencies) associated to the rotational speed of the rotor. The influence of the rotational speed on the rotor natural frequencies increases when the gyroscopic effect is more significant.

Unbalance Response of the System

The external forces that act on the system, as a result of the mass unbalance $\{F_d\}$, and the corresponding response $\{q_d\}$ in relation to that excitation force can be written in the following way:

$$\{F_d\}=\{f_c\}Cos(\Omega t)+\{f_s\}Sin(\Omega t)\ ;\ \ \{q_d\}=\{q_c\}Cos(\Omega t)+\{q_s\}Sin(\Omega t) \qquad (18)$$

Substituting $\{q_d\}$and its derivatives into equation (16) and assuming that the unbalance external forces ($\{F_d\}=\{F_e\}$) are known, $\{q_c\}$ and $\{q_s\}$ vectors can be determined from the following equation:

$$\begin{Bmatrix}\{q_c\}\\ \{q_s\}\end{Bmatrix}=\begin{bmatrix}[K]-\Omega^2[M] & \Omega[\Omega[G]+[C]]\\ -\Omega[\Omega[G]+[C]] & [K]-\Omega^2[M]\end{bmatrix}^{-1}\begin{Bmatrix}\{f_c\}\\ \{f_s\}\end{Bmatrix} \qquad (19)$$

The system response to the mass unbalance is obtained in the time domain by the equation that defines $\{q_d\}$and, in this case, the mass unbalance is considered as known.

Computational Software

Computational software to solve the system of matricial equations (16) and (17) was written in FORTRAN 90. The software flow chart is given in Fig. 6. This program allows the analysis of the influences of the considerations made in the different modelling processes of the coupling in the mechanical system through the Campbell Diagram. The software also allows the analysis of the unbalance response of the system. The global matrices of the system were assembled from the partial matrices of the mechanical components of the system. From the matricial equation solution using the Direct Method described by Nelson and Crandall [5], the Campbell Diagram was elaborated and the unbalance response of the system was evaluated. Software for the model fitting was also developed. The procedure consists of adjusting the simulation results to experimental data, using the minimum quadratic technique. In this way, it is possible to verify the model performance and some sensitivity of the parameters.

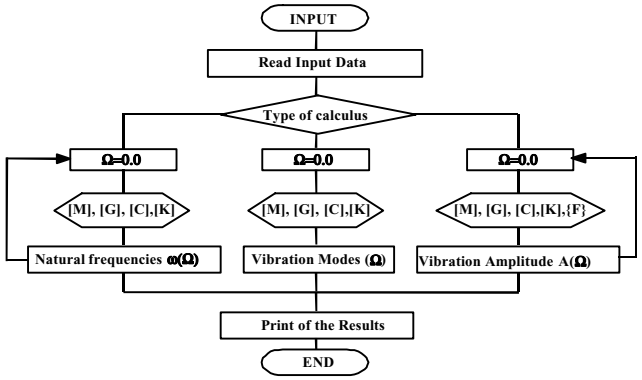

Figure 6. Flow Chart of the PROGRA_M1.mdp Software.

Numerical Simulation

A mechanical system was elaborated to perform the complete methodology, Sekhar et al (1996) [7], as shown in Fig. 7. Such a system analyses the influence of the different flexible coupling models on the natural frequencies, as well as the unbalance response of the system.

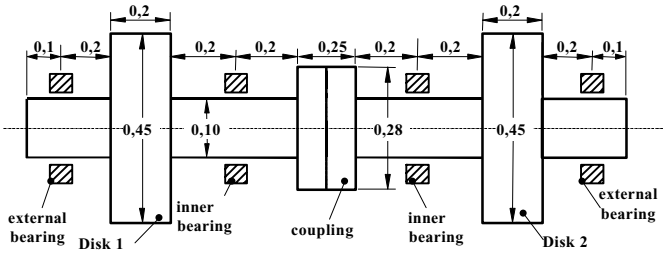

Figure 7. Simulated Mechanical System [geometric dimensions in meters].

The following cases were simulated in the program:

. Case I: When the coupling is modelled as a rigid disk according to the general approach. In this case the system is modelled with 8 beam elements, 3 rigid disks, and 4 bearings;

. Case II: When the coupling is modelled with the first approach of Kramer [3]. In this case, the model presents two nodes and its constraints comply with the degrees of freedom established by the model, and two masses of the disks in each node of the coupling, which include the inertia of the coupling;

. Case III: It corresponds to the second model suggested by Kramer [3] and it is similar to case II. The only difference is that the rotational stiffness and damping of the coupling are included;

. Case IV: When the coupling is modelled in agreement with the first model proposed by Nelson and Crandall [5], in which the translational and rotational stiffness, as well as the inertia of the coupling are considered. The system was discretized in 10 nodes, 8 beam elements, 2 rigid disks, and 4 bearings;

. Case V: It corresponds to the second model defined by Nelson and Crandall [5]. This model is similar to that of case IV. The difference is that the translational and rotational damping of the coupling are added.

Table (1) presents the corresponding physical and dynamic characteristic data of the components of the hypothetical mechanical system indicated in Fig. 7, based on Sekhar et al (1996) [7], for a previous verification of the dynamic response considering the five coupling models proposed.

Fig. 8a1-a2, Fig. 8b1-b2, Fig. 9a1-a2, and Fig. 9b1-b2 are the Campbell diagrams for the first four natural frequencies. In this case study, the 1st and 3rd natural frequencies are model-dependent while

the 2nd and the 4th are not. This fact is due to the modal shape of the complete system associated to these frequencies. In the 2nd and 4th natural frequencies there is no significant displacement at the couplings, so that its model does not affect the Campbell Diagram, which is coincidental for all models analysed. In the 1st and 3rd natural frequencies, the contribution of the coupling displacements is highlighted in the Campbell Diagram, as the models start and continue to present different natural frequencies in the whole range of rotational speed. Notice that the 2nd Kramer, 1st and 2nd Nelson and Crandall models are coincidental in Fig. 8a2, 8b2, 9a2 and 9b2. The rigid models and the 1st Kramer model are quite different in Fig. 8a1 and 9a1 and very close in Fig. 8b1 and 9b1.

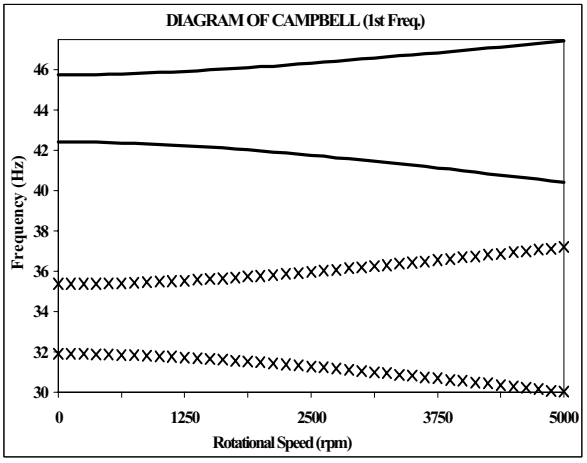

(a1)

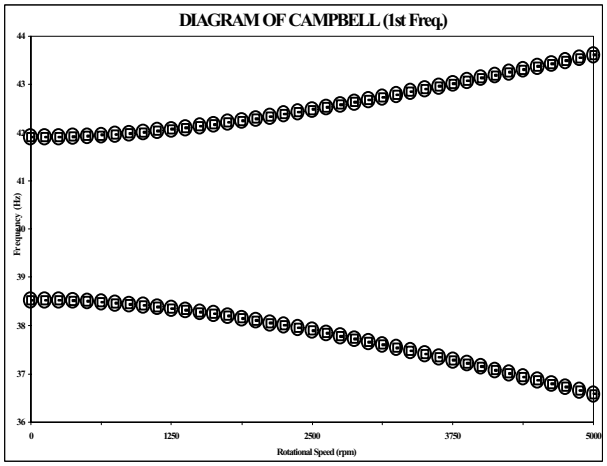

(a2)

Figure 8. Variation of the natural frequencies of the system with the rotational speed for the five cases analysed: (a1 and a2) first natural frequency of the system; (b1 and b2) second natural frequency of the system. (— Rigid; × Kramer1; ···Kramer2; Nelson_Crandall1; O Nelson_Crandall2).

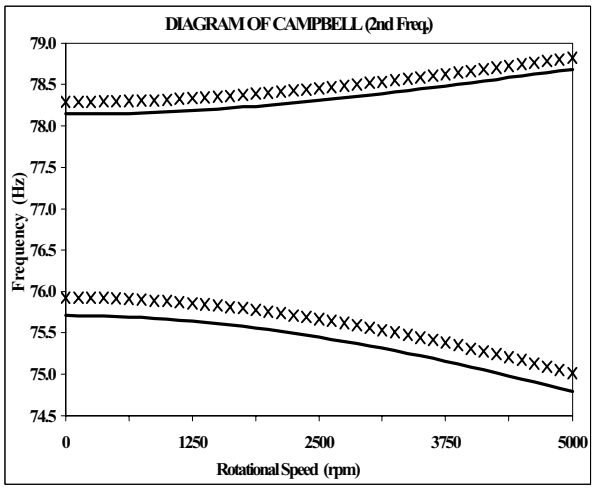

(b1)

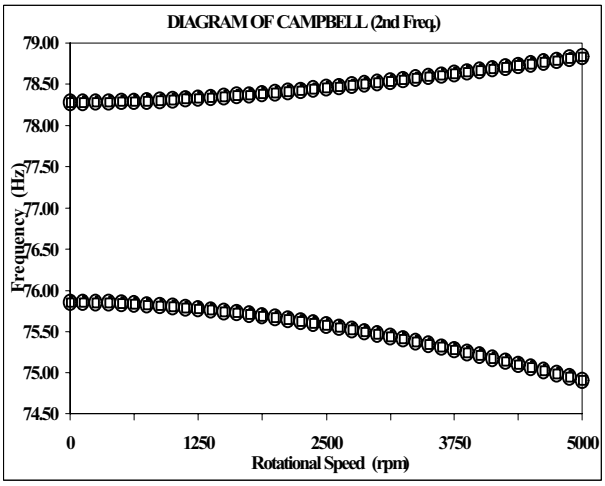

(b2)

Figure 8. (Continued).

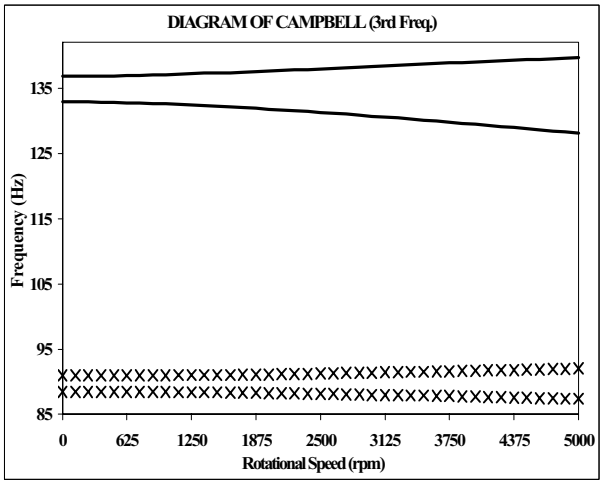

(a1)

Figure 9. Variation of the natural frequencies of the system with the rotational speed for the five cases analysed: (a1 and a2) third natural frequency of the system; (b1 and b2) fourth natural frequency of the system. (— Rigid; × Kramer1; ···Kramer2; Nelson_Crandall1; O Nelson_Crandall2).

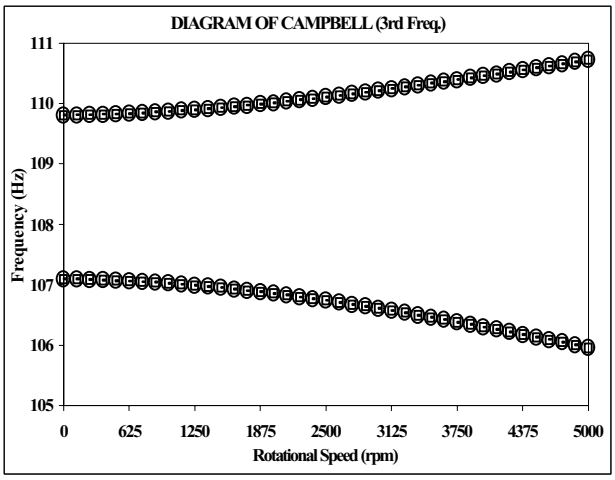

(a2)

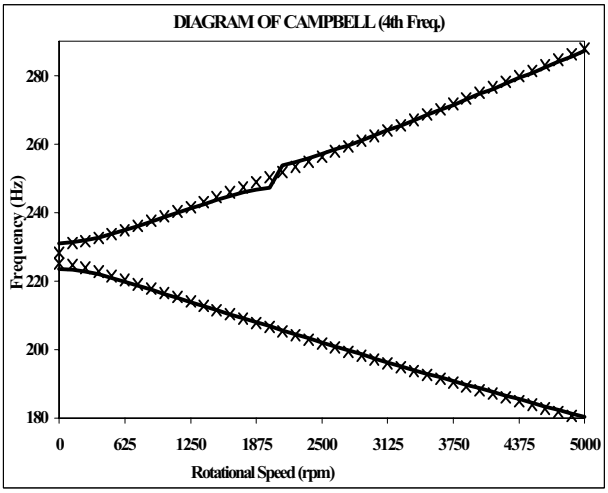

(b1)

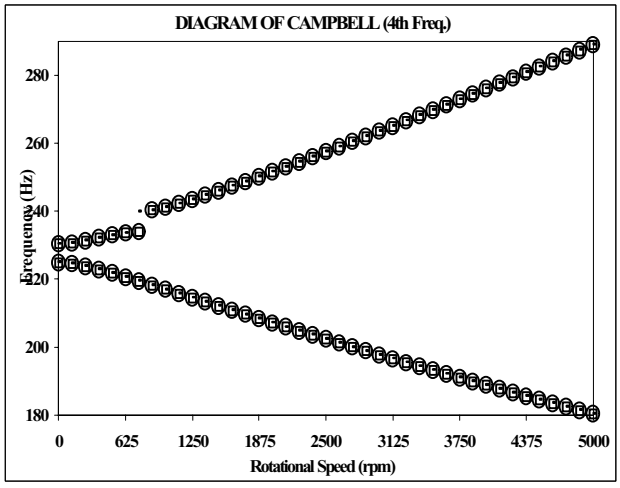

(b2)

Figure 9. (Continued).

Besides that, Fig. 10a1-a2, 10b1-b2, 11a1-a2 and 11b1-b2 represent the unbalance response, in the X and Z directions for the shaft, located in Disk 1 of the system. These unbalance responses were caused by the mass unbalance in Disk 1, roughly around 0.00189 kgm at a phase angle of 0^o from the Z axis. The frequency range is close to the resonance frequencies, excited by the residual mass unbalancing. This analysis holds for the five cases mentioned above.

Notice that the rigid and 1st Kramer models are quite different in Fig. 10a1, 10b1, 11a1 and 11b1. Otherwise, 2nd Kramer, 1st and 2nd Nelson and Crandall models are quite coincidental in Fig. 10a2, 10b2, 11a2 and 11b2 as these models contain rotational and translational coefficients.

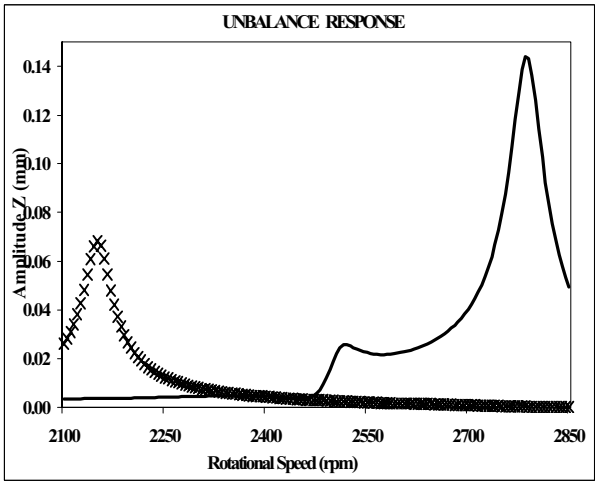

(a1)

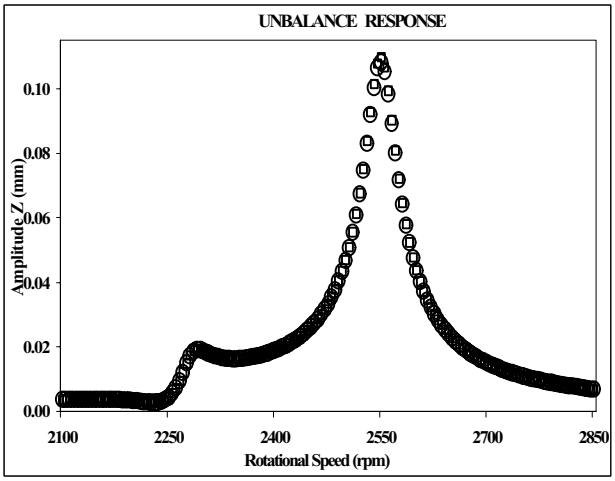

(a2)

Figure 10. Unbalance Response of Disk1 close to the first resonance condition: (a1 and a2).direction Z; (b1 and b2) direction X. (◆ Measured; — Rigid; × Kramer1; ···Kramer2; Nelson_Crandall1; O Nelson_Crandall2).

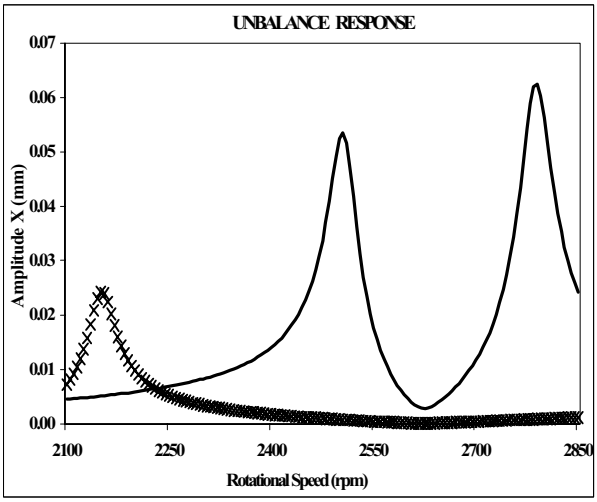

(b1)

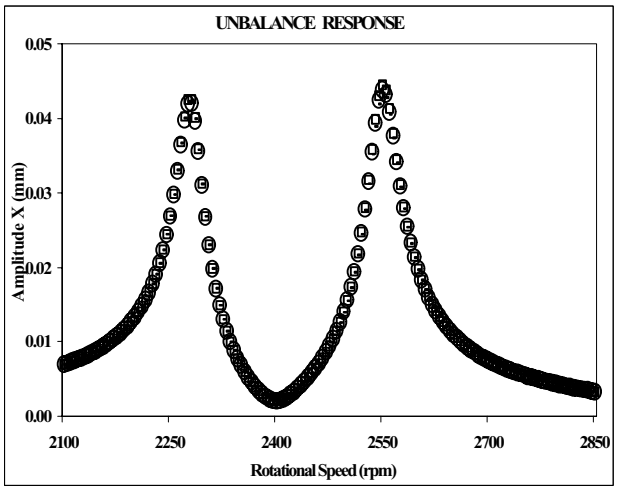

(b2)

Figure 10. (Contniued).

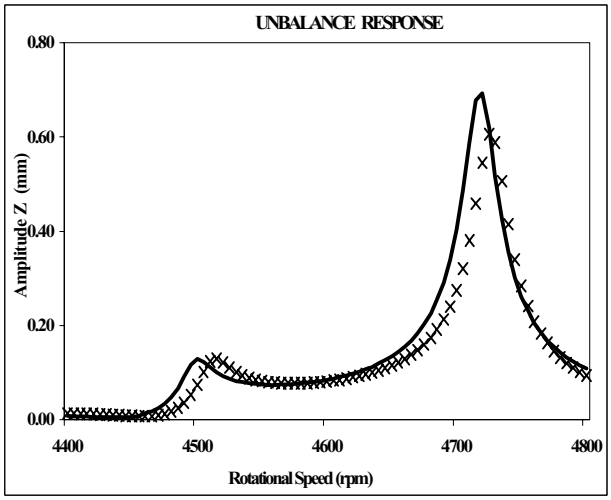

(a1)

Figure 11. Unbalance Response of Disk1 close to the second resonance condition: (a1 and a2).direction Z; (b1 and b2) direction X. (◆ Measured; — Rigid; × Kramer1; ⋯Kramer2; Nelson_Crandall1; O Nelson_Crandall2).

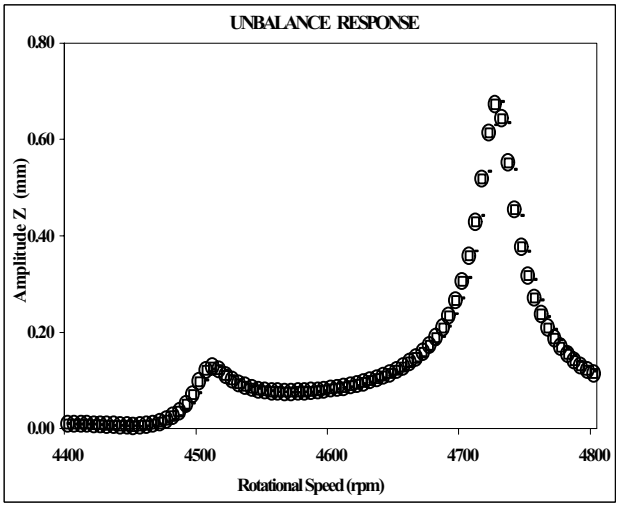

(a2)

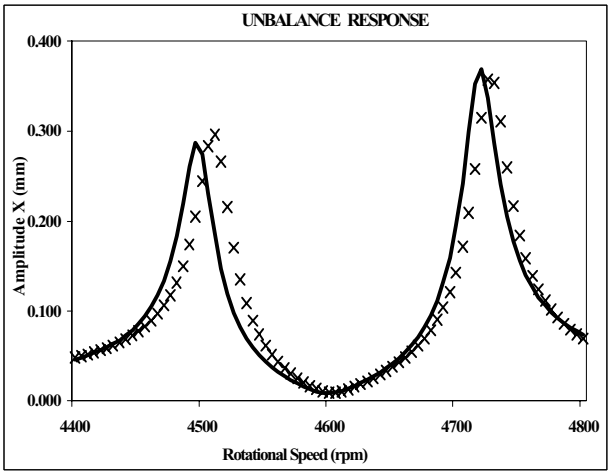

(b1)

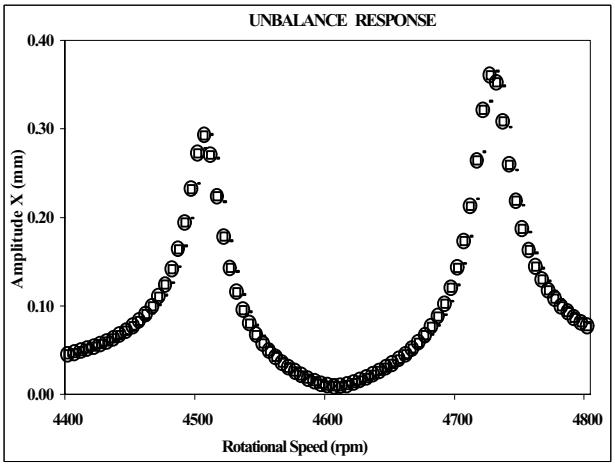

(b2)

Figure 11. (Contniued).

Model Updating

Most of the model updating methods proposed in literature consist of evaluating the natural frequencies and vibration modes in terms of the mass ΔM and stiffness ΔK matrix variations. ΔM and ΔK can be calculated by inverse sensitivity starting from the difference between measured and calculated modal parameters [10]

[11]. But the understanding about the meaning of the ΔM and ΔK changes in terms of physical variations of the structural parameters is still not solved. In that sense, the present work presents the application of a fitting method to the FEM (Finite Element Method) of the rotor-bearings-coupling system. The method uses an unbalance FRF (Frequency Response Function) of the system as a fitting curve. The restricted modified minimum square method for non-linear estimation of parameters, well known as the Levenberg-Marquart Algorithm, is used, where the main variables are defined below. The objective function to be minimised and the constrains are given by:

$$F = \frac{1}{2}\{frf_i\}^T\{frf_i\} \quad Li \le Xp \le Ls \tag{20}$$

Where: Li is the lower limit, Ls is the upper limit, Xp is the fitting parameter and frf_i is the frequency response function used as input to minimise the objective function [12].

$$frf_i = \left(20 * Log_{10}\left|FRF_{mi}\right| - 20 * Log_{10}\left|FRF_{ei}\right|\right) \Big/ 1.0 * 10^{-4} \tag{21}$$

FRF_{mi} is the i-th component of the experimental unbalance response of the rotor, simulated with FEM and a noise formulation given in equation (22) [13]:

$$FRE_{mi} = FRE_{ei} + FRE_{ei} * \frac{\beta_a}{100} * rand[-1,1] + \sqrt{\sum_{j=1}^{j=np} FRE_{ej}^2 \Big/ np} * \frac{\beta_s}{100} * rand[-1,1] \tag{22}$$

FRF_{ei} is the i-th component of the simulated unbalance response at each step of interaction, np is the FRF number of points, βa is the random error factor (10%) and βs is the systematic error factor (1%).

The search direction is:

$$\vec{d} = \left([J]_{m,n}^T * [J]_{m,n} + \mu * [I]_{n,n}\right)^{-1} * [J]_{m,n}^T * \{frf\}_{m,1} \tag{23}$$

$[J]_{n.m}$ is the Jacobian matrix, [I] is the identity matrix, μ is the Levenberg-Marquardt parameter, m is the FRF number of points and n is the number of parameters to be fitted.

The Jacobian matrix is evaluated using the finite difference method:

$$[J]_{m,n} = \left[J_{ij}\right]_{m,n} ; J_{ij} = \frac{\partial(frf_i)}{\partial X_j} ; \; i = 1,..., m ; j = 1,..., n \tag{24}$$

Examples

The models to be fitted correspond to the mechanical system of Fig. 7, proposed by Sekhar et al (1996) [7]. At this point, an experimental unbalance response is simulated in the following way: The FEM program calculates the unbalance FRFs in the coupling position (d.o.f. 17,18,19,20), considering the second Nelson and Crandall model (K_T=1.2x10^6 N/mm, K_R=1.35791x10^9 Nmm/rad, C_T=1.13 x10^{-2} Ns/mm, C_R=1.13 x10^4 Nmms/rad as shown in Table 1). Once the simulated response is obtained, the experimental response is defined applying equation (22). In Tables 1 and 2, each d.o.f. corresponds to a node displacement of the coupling (radial or angular) and there are four degrees of freedom for each node (two radial d.o.f.-17 and 18 and two angular d.o.f.-19 and 20). In this way, the program generates the curves to be fitted in function of some parameters. The parameters correspond to the coupling model represented as stiffness and damping coefficients. However, in the model that considers a rigid coupling, the stiffness and damping coefficients will be fitted to the inner bearings closer to the coupling [14].

Table 1. Physical and Dynamical Properties of the components of the simulated mechanical system.

DISKS		SHAFTS
Disk1: Mass Density 7800kg/m^3	Disk2: Mass Density 7800kg/m^3	Density 7800 kg/m^3 , Young Modulus 2*10^{11}N/m^2 , Poisson Coefficient 0.3 , Shear Factor 0.9

EXTERNAL BEARINGS		INNER BEARINGS	
1	Stiffness: Kxx=10^{8}N/m, Kxz=0, Kzz=1.5*10^{8}N/m, Kzx=0	1	Stiffness: Kxx=10^{7}N/m, Kxz=0, Kzz=1.5*10^{7}N/m, Kzx=0
	Damping: Cxx=0.5*10^{3}Ns/m,Cxz=0,Czz=0.8*10^{3}Ns/m,Czx=0		Damping: Cxx=10^{3}Ns/m,Cxz=0,Czz=10^{3}Ns/m,Czx=0
2	Stiffness: Kxx=10^{7}N/m, Kxz=0, Kzz=10^{7}N/m, Kzx=0	2	Stiffness: Kxx=10^{7}N/m, Kxz=0, Kzz=1.5*10^{7}N/m, Kzx=0
	Damping: Cxx=10^{3}Ns/m,Cxz=0,Czz=10^{3}Ns/m,Czx=0		Damping: Cxx=10^{3}Ns/m,Cxz=0,Czz=1.1*10^{3}Ns/m,Czx=0

COUPLING (Kramer)	COUPLING (Nelson and Crandall)
Mass Density 7800kg/m^3	Mass Density 7800kg/m^3
Rotational Stiffness 13579.1*10^2 Nm/rad	Rotational Stiffness 13579.1*10^2 Nm/rad; Translational 1.2*10^9 N/m
Rotational Damping 11.3 Nms/rad	Rotational Damping 11.3 Nms/rad; Translational 11.3 Ns/m

Table 2. Fitted curves results for the first and second Nelson and Crandall's model and the second Kramer's model.

Parameters		2nd KRAMER		1st NELSON and CRANDALL		2nd NELSON and CRANDALL	
	Starting point	**1 d.o.f.**	**4 d.o.f.**	**1 d.o.f.**	**4 d.o.f.**	**1 d.o.f.**	**4 d.o.f.**
K_T	0.60E+6	---	---	979469826.34	35221.00	186206.03	1393514407.12
K_R	0.678955E+9	355413905.74	1337815799.83	1355628502.13	1362140288.76	1358700314.64	1337822632.58
C_T	0.565E-2	---	---	---	---	545.97	.00304427
C_R	0.565E+4	10711.50	.000	---	---	.00000003	.0000000
# Interations		16	13	19	23	42	18
Error		1.301286	2.456724	1.360356	2.724172	1.310202	2.456405

Two cases were analyzed:

Case 1. The optimisation process uses an unbalance response corresponding to d.o.f. number 17 of the coupling in the X direction, in the 2000 to 3000 rpm range. The five models proposed for the rotor-bearing-coupling system were fitted with the following considerations: the first and second Nelson and Crandall models, as well the second Kramer model were fitted based on the stiffness and damping coefficients of the coupling. The rigid coupling model and the first Kramer model were fitted based on the stiffness and damping parameters of the two bearings next to the coupling. The only constrain is that the fitted parameters must be positive, and the starting unbalance response curve is about 50% lower than the experimental curve.

The results obtained in each updating process of the unbalance response curves and fitting parameter methods are described in Tables 2 and 3. Fig. 12a presents the fitted unbalance response curves at the corresponding d.o.f.17 used in the process for rigid and 1st Kramer models. Fig. 12b presents the fitted unbalance response curves at the corresponding d.o.f.17 used in the process for 2nd Kramer, 1st and 2nd Nelson Crandall models.

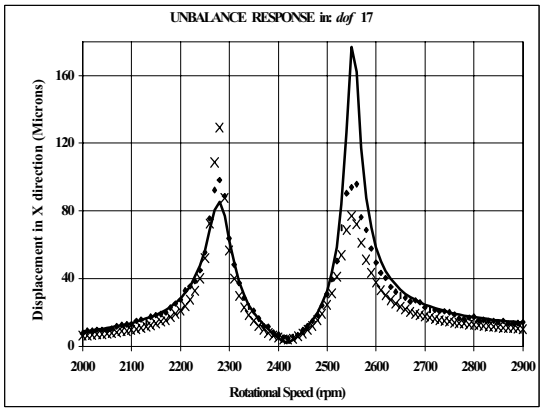

(a)

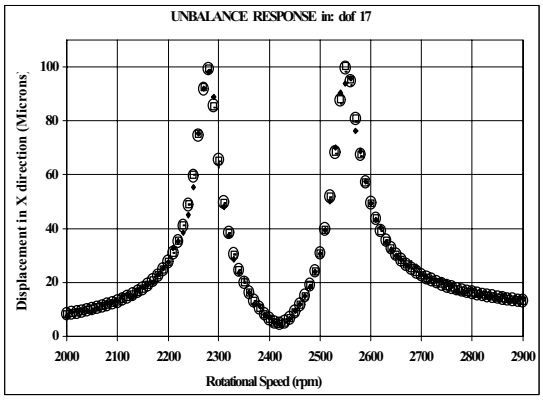

(b)

Figure 12. FRF fitted curves in X direction of the coupling (d.o.f. 17): (a)rigid and 1st Kramer models; (b) 2nd Kramer, 1st and 2nd Nelson and Crandall models. (◆ Measured; — Rigid; × Kramer1; ⋯Kramer2; Nelson_Crandall1; O Nelson_Crandall2).

Case 2. The optimisation process uses the unbalance response corresponding to d.o.f. numbers 17, 18, 19 and 20 of the coupling, respectively in X, Z, αx and αz directions, in the 2000 to 3000 rpm range. The models considered in the simulation, as well as the constrains and the starting curves have the same considerations presented in case 1. The obtained results in each updating process are described in Tables 2 and 3. The final fitted unbalance responses are presented in Fig. 13a and 13b for d.o.f. 17 and 18 (translation coordinates); and Fig. 14a and 14b are the fitted responses for d.o.f. 19 and 20 (bending angles). The number of points corresponds to the number of frequencies plotted for each d.o.f. onto the 2000-2900 rpm frequency range (98 points for d.o.f. 17 and 98 points for d.o.f. 18) as well as for d.o.f. 19 and 20.

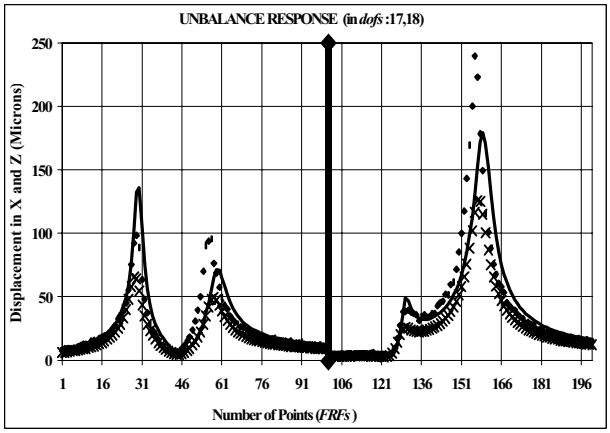

(a)

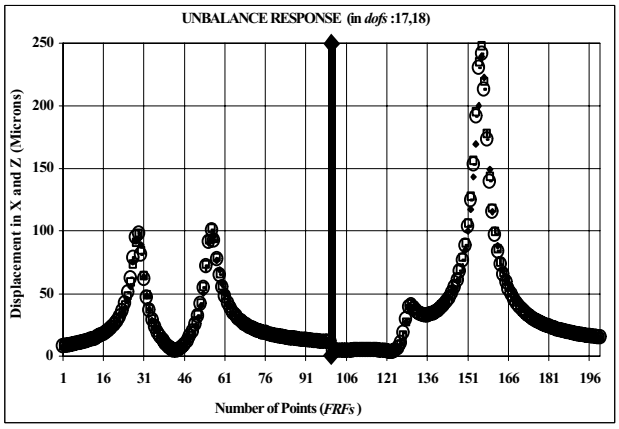

(b)

Figure 13. Fitted curves in X and Z directions of the coupling (d.o.f. 17 and 18): (a)rigid and 1st Kramer models; (b) 2nd Kramer, 1st and 2nd Nelson and Crandall models. (◆ Measured; — Rigid; × Kramer1; ⋯Kramer2; Nelson_Crandall1; O Nelson_Crandall2).

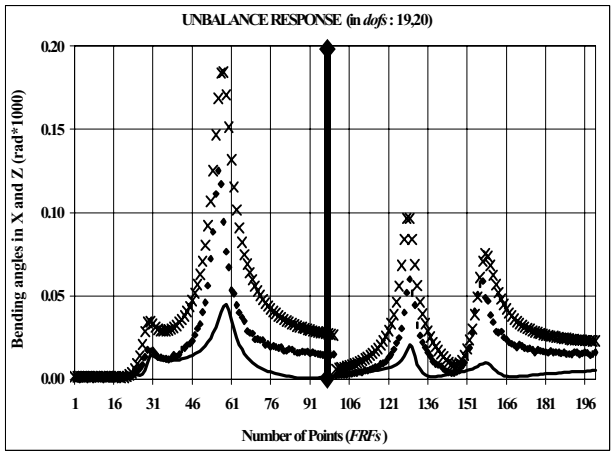

(a)

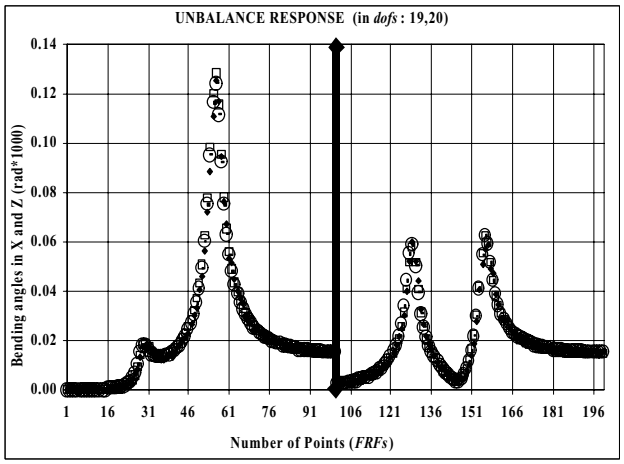

(b)

Figure 14. Fitted curves in αX and αZ directions of the coupling (d.o.f. 19 and 20): (a)rigid and 1st Kramer models; (b) 2nd Kramer, 1st and 2nd Nelson and Crandall models. (◆ Measured; — Rigid; × Kramer1; ···Kramer2; Nelson_Crandall1; O Nelson_Crandall2).

Conclusions

The FEM of the rotor-bearings-coupling system [6,8,9] analyses the bending vibrations of the system. Fig. 8a and 9a show how the values of the first and third natural frequencies of the system differ so much on the direct whirl as well as on the retrograde whirl effect. Certainly, the effect depends on the considered model as well as on the modal shape of the rotor. Fig. 8a2 and 8b2 and 9a2 and 9b2 show that the difference between the second and fourth natural frequencies is not significant in this case, because there is no significant contribution of the coupling to these modes. Analysing the unbalance responses in Fig. 10a1, 10a2, 10b1 and 10b2 that represent the vibration amplitudes in the Z (a1 and a2) and X (b1 and b2) directions, in the first resonance condition, it is possible to observe the same effect of the Campbell Diagram for the first natural frequency of the system, which means that the resonance positions change depending on the considered model. This can be attributed to the Kramer model that comprises the rotational stiffness and damping parameters and the Nelson and Crandall's models, that include the translational stiffness and damping as well. Also, depending on those parameters, some frequencies can be less sensitive. In this way, the coupling model influence on the rotating mechanical systems can significantly affect the natural frequencies and the corresponding vibration amplitudes. Besides that, according to the existing approaches in literature towards coupling modelling, the natural frequencies and the response of the system will be different, depending on the real mechanical system analysed. An experimental curve was generated using the most complete model (2nd Nelson and Crandall model) with an random noise of 10%. Also in this case, the coupling parameters do not converge to the original values used in the simulation during the optimisation process. The only fitted parameter was the rotational stiffness KR with an error of 1.5% approximately. However, the fitting errors showed in Table 2 are smaller than the errors of Table 1 for rigid coupling models. Fig. 12, 13 and 14 show that experimental fitting is reached with success for the five models proposed in the work, with the difference that the fittings tend to be better for the flexible models than for the rigid models of the coupling (Fig. 12b, 13b and 14b). In this sense, the best fittings correspond to the first and second Nelson and Crandall models and the second Kramer model, as indicated by the fitting errors in Table 2 and Table 3. It is also important to point out that some fitted parameters converged for null values. This fact suggests that the degrees of freedom associated to these parameters are not very significantly influenced by the coupling coefficients. As a final conclusion, in the parameter estimation process of the mechanical systems, a parametric sensitivity analysis is of significant importance for the choice of the unbalance response and the d.o.f to be used in the process. The next step is the experimental model updating of the flexible coupling parameters of stiffness and damping coefficients.

Table 3. Fitted curves results for the rigid coupling model and the first Kramer's model.

Parameters		Rigid Coupling		1st KRAMER	
	Starting point	**1 d.o.f.**	**4 d.o.f.**	**1 d.o.f.**	**4 d.o.f.**
K_{XX}	01.00e+04	4923.01	4974.05	20495.45	20307.43
K_{ZZ}	01.00E+04	4820.28	5451.16	20675.82	21274.49
C_{XX}	01.00E+00	1.43	.42	.00	1.93
C_{ZZ}	01.00E+00	.000	1.80	1.66	2.84
# Interations		66	17	23	58
Error		12.577670	13.092020	7.624786	14.148430

Acknowledgements

The authors would like to thank the Brazilian institutions CNPq, FAPESP, and UNICAMP for their financial support for this work and Prof. Dr. J.R.F. Arruda for the valuable discussions.

References

[1] Ehrich,F.F., 1992, " Handbook of Rotordynamics" , USA, McGRAW-HILL Inc., pp.2.1-2.25.

[2] Gibbons, C. B., 1976, "Coupling Misalignment Forces" Proceedings of the fifth Turbomachinery Symposium, Gas Turbine Laboratories, Texas A & M University College Station, Texas, pp. 111-116.

[3] Kramer., E., 1993, "Dynamics of Rotors and Foundations", New York, Springer-Verlag. pp. 381.

[4] Lalanne M., Ferraris G., 1990, "Rotordynamics Prediction in Engineering", New York, John Wiley & Sons Ltd. pp. 197.

[5] Nelson, H. D. & Crandall, S. H., "Analytic Prediction of Rotordynamic Response". In: EHRICH, F. F., Handbook of rotordynamics. United States of America, McGraw-Hill, Inc., 1992. Cap2., p. 2.1-2.84.

[6] Nelson, H. D., McVaugh, J. M., 1976, "Dynamics of Rotor–Bearing Systems Using Finite Elements", ASME Journal of Engineering for Industry, Vol. 98, pp. 593-600.

[7] Sekhar, A. S., Rao, A. S., 1996, "Vibration analysis of Rotor–Coupling–Bearing System with Misaligned Shafts". International Gas Turbine and Aeroengine Congress & Exhibition.

[8] Tapia, T. A., Lucchesi, C. K., 2000, "Efeito dos Acoplamentos nos Rotores Horizontais", 9º Congreso Chileno de Ingeniería Mecánica, IV Congreso Nacional de Energía, Valparaíso, Chile.

[9] Xu, M., Marangoni, R. D., 1994, "Vibration Analysis of a Motor-Flexible Coupling-Rotor System Subject to Misalignment and Unbalance", Part I: Theorical model and analysis, Part II: Experimental validation. Journal of Sound and Vibration, Vol. 176, pp. 663-691.

[10] Ewins, D.J., 1984, "Modal Testing Theory and Practice", RSP John Wiley, Letchworth.

[11] O' Callahan, J.C., Leung, R.K., 1986, "Optimisation of Mass and Stiffness Matrices Using a Generalized Inverse Technique on the Measured Modes", Proceedings of the 4th IMAC, Orlando, 1986, pp. 409-413.

[12] Dos Santos, J.M.C., Ferraz, F.G., 2001, "Block-Krylov Component Synthesis and Minimum Rank Perturbation Theory for Damage Detection in Complex Structures", Proceedings of the IX DINAME, 5-9 March 2001, Florianópolis-SC-Brazil, pp. 329-334.

[13] Arruda, J.R.F., Duarte, M.A.V., 1993, "Updating Rotor-Bearing Finite Element Models Using Experimental Frequency Response Functions", RBCM-J. of the Braz. Soc. Mechanical Sciences, Vol. XV, nº 2, 1993, pp. 136-149.

[14] Tadeo A.T., Cavalca K.L. "Modeling effect of flexible and rigid couplings in mechanical systems", IFToMM2002 – 6th International Conference on Rotordynamics, VOL.1, Sydney – Australia, 2002, pp. 420-429.